

High-speed optical modulation based on carrier depletion in a silicon waveguide

Ansheng Liu¹, Ling Liao¹, Doron Rubin², Hat Nguyen¹, Berkehan Ciftcioglu¹, Yoel Chetrit², Nahum Izhaky², and Mario Paniccia¹

¹Intel Corporation, 2200 Mission College Blvd, SC12-326, Santa Clara, CA 95054

²Intel Corporation, S. B. I. Park Har Hotzyim, Jerusalem, 91031, Israel

Ansheng.liu@intel.com

Abstract: We present a high-speed and highly scalable silicon optical modulator based on the free carrier plasma dispersion effect. The fast refractive index modulation of the device is due to electric-field-induced carrier depletion in a Silicon-on-Insulator waveguide containing a reverse biased pn junction. To achieve high-speed performance, a travelling-wave design is used to allow co-propagation of electrical and optical signals along the waveguide. We demonstrate high-frequency modulator optical response with 3 dB bandwidth of ~20 GHz and data transmission up to 30 Gb/s. Such high-speed data transmission capability will enable silicon modulators to be one of the key building blocks for integrated silicon photonic chips for next generation communication networks as well as future high performance computing applications.

©2007 Optical Society of America

OCIS codes: (250.7360) Waveguide modulators; (060.4080) Modulation; (203.7370) Waveguides; (250.5300) Photonic integrated circuits.

References and Links

1. A. Liu, R. Jones, L. Liao, D. Samara-Rubio, D. Rubin, O. Cohen, R. Nicolaescu, M. Paniccia, "A high-speed silicon optical modulator based on a metal-oxide-semiconductor capacitor," *Nature* **427**, 615-618 (2004).
2. L. Liao, D. Samara-Rubio, M. Morse, A. Liu, H. Hodge, D. Rubin, U. D. Keil, T. Franck, "High-speed silicon Mach-Zehnder modulator," *Opt. Express* **13**, 3129-3135 (2005).
3. A. Huang, G. Gunn, G.-L. Li, Y. Liang, S. Mirsaidi, A. Narasimha, T. Pinguet, "A 10 Gb/s photonic modulator and WDM MUX/DEMUX integrated with electronics in 0.13 μ m SOI CMOS," in *Technical Digest of 2006 IEEE International Solid-State Circuits Conference, Session 13/ Optical Communication/13.7*.
4. S. J. Koester, G. Dehlinger, J. D. Schaub, J. O. Chu, Q. C. Ouyang, A. Grill, "Germanium-on-insulator photodetectors," in *Technical Digest of 2005 2nd IEEE International Conference on Group IV Photonics*, pp. 171-173.
5. M. Oehme, J. Werner, E. Kasper, M. Jutzi, M. Berroth, "High bandwidth Ge p-i-n photodetector integrated on Si," *Appl. Phys. Lett.* **89**, 071117-071117-3 (2006).
6. O. Boyraz, B. Jalali, "Demonstration of a silicon Raman laser," *Opt. Express* **12**, 5269-5273 (2004).
7. H. Rong, *et. al.* "A continuous-wave Raman silicon laser," *Nature* **433**, 725-728 (2005).
8. A. Liu, H. Rong, M. Paniccia, O. Cohen, D. Hak, "Net optical gain in a low loss silicon-on-insulator waveguide by stimulated Raman scattering," *Opt. Express* **12**, 4261-4268 (2004).
9. O. Boyraz, B. Jalali, "Demonstration of 11 dB fiber-to-fiber gain in a silicon Raman amplifier," *Electron. Express* **1**, 429-434 (2004).
10. Q. Xu, V. R. Almeida, M. Lipson, "Demonstration of high Raman gain in a submicrometer-size silicon-on-insulator waveguide," *Opt. Lett.* **30**, 35-37 (2005).
11. R. Jones, *et. al.* "Net continuous-wave optical gain in a low loss silicon-on-insulator waveguide by stimulated Raman scattering," *Opt. Express* **13**, 519-525 (2005).
12. R. L. Espinola, J. I. Dadap, R. M. Osgood, Jr., S. J. McNab, Y. A. Vlasov, "C-band wavelength conversion in silicon photonic wire waveguides," *Opt. Express* **13**, 4341-4349 (2005).
13. K. Yamada, *et. al.* "All-optical efficient wavelength conversion using silicon photonic wire waveguide," *IEEE Photon. Technol. Lett.* **18**, 1046-1048 (2006).
14. H. Rong, Y. H. Kuo, A. Liu, M. Paniccia, O. Cohen, "High efficiency wavelength conversion of 10 Gb/s data in silicon waveguides," *Opt. Express* **14**, 1182-1188 (2006).
15. A. W. Fang, H. Park, O. Cohen, R. Jones, M. Paniccia, J. E. Bowers, "Electrically pumped hybrid AlGaInAs-silicon evanescent laser," *Opt. Express* **14**, 9203-9210 (2006).
16. K. Noguchi, O. Mitomi, H. Miyazawa, "Millimeter-wave Ti:LiNbO₃ optical modulators," *J. Lightwave Technol.* **16**, 615-619 (1998).

17. K. Tsuzuki, T. Ishibashi, T. Ito, S. Oku, Y. Shibata, T. Ito, R. Iga, Y. Kondo, Y. Tohmori, "A 40-Gb/s InGaAlAs-InAlAs MQW n-i-n Mach-Zehnder modulator with a drive voltage of 2.3 V," *IEEE Photon. Technol. Lett.* **17**, 46-48 (2005).
18. R. A. Soref, P. J. Lorenzo, "All-silicon active and passive guided-wave components for $\lambda=1.3$ and $1.6 \mu\text{m}$," *IEEE J. Quantum Electron.* **QE-22**, 873-879 (1986).
19. R. A. Soref, B. R. Bennett, "Electrooptical effects in silicon," *IEEE J. Quantum Electron.* **QE-23**, 123-129 (1987).
20. R. S. Jacobsen, *et al.* "Strained silicon as a new electro-optic material," *Nature* **441**, 199-202 (2006).
21. Y.-H. Kuo, Y. K. Lee, Y. Ge, S. Ren, J. E. Roth, T. I. Kamins, D. A. B. Miller, J. S. Harris, "Strong quantum-confined Stark effect in germanium quantum-well structures on silicon," *Nature* **437**, 1334-1336 (2005).
22. C. K. Tang, G. T. Reed, "Highly efficient optical phase modulator in SOI waveguides," *Electron. Lett.* **31**, 451-452 (1995).
23. F. Y. Gardes, G. T. Reed, N. G. Emerson, C. E. Png, "A sub-micron depletion-type photonic modulator in Silicon on Insulator," *Optics Express* **13**, 8845-8853 (2006).
24. Q. Xu, B. Schmidt, S. Pradhan, M. Lipson, "Micrometre-scale silicon electro-optic modulator," *Nature* **435**, 325-327 (2005).
25. F. Gan, F. X. Kartner, "High-speed silicon electrooptic modulator design," *IEEE Photon. Technol. Lett.* **17**, 1007-1009 (2005).
26. A. Alping, X. S. Wu, T. R. Hausken, and L. A. Coldren, "Highly efficient waveguide phase modulator for integrated optoelectronics," *Appl. Phys. Lett.* **48**, 243-245 (1986).
27. J. G. Mendoza-Alvarez, L. A. Coldren, A. Alping, R. H. Yan, T. Hausken, K. Lee, and K. Pedrotti, "Analysis of depletion edge translation lightwave modulators," *IEEE J. Lightwave Technol.* **6**, 793-807 (1988).
28. R. C. Alferness, "Waveguide electrooptic modulators," *IEEE Trans. Microwave Theory Tech.* **30**, 1121-1137 (1982).
29. R. G. Walker, "High-speed III-V semiconductor intensity modulators," *IEEE J. Quantum Electron.* **27**, 654-667 (1991).
30. S. L. Chuang, *Physics of Optoelectronics Devices*. (John Wiley, New York, 1995).
31. G. T. Reed, A. P. Knights, *Silicon Photonics: an introduction* (John Wiley, Chichester, 2004).
32. K. Tsuzuki, K. Sano, N. Kikuchi, N. Kashio, E. Yamada, Y., Shibata, T. Ishibashi, M. Tokumitsu, and H. Yasaka, "0.3 V_{pp} single-drive push-pull InP Mach-Zehnder modulator module for 43-Gbit/s systems," in *Technical Digest of 2006 Optical Fiber Communication Conference and National Fiber Optic Engineers Conference 5-10 March 2006*, p.3.
33. Y. Cui and P. Berini, "Modeling and design of GaAs traveling-wave electrooptic modulators based on capacitively loaded coplanar strips," *IEEE J. Lightwave Technol.* **24**, 544-554 (2006).
34. S. Pae, T. Su, J. P. Denton, G. W. Neudeck, "Multiple layers of silicon-on-insulator islands fabrication by selective epitaxial growth," *IEEE Electron Device Lett.* **20**, 194-196 (1999).

1. Introduction

Silicon photonics has recently become a subject of intense interest because it offers an opportunity for low cost optoelectronic solutions for applications ranging from telecommunications down to chip-to-chip interconnects. In the past few years, there have been significant advances in pushing device performance of CMOS-compatible silicon building blocks needed for developing silicon integrated photonic circuits. Fast silicon optical modulators [1-3], SiGe photo-detectors [4, 5], silicon Raman lasers [6, 7], silicon optical amplifiers [8-11], silicon wavelength converters [12-14], and hybrid silicon lasers [15] have been demonstrated. Nevertheless, the fastest demonstrated data transmission using a silicon modulator so far is ~ 10 Gb/s [2, 3]. In order to meet the ever-increasing bandwidth demand of next generation communication networks and future high performance computing applications, it would be desirable to have significantly faster ($\gg 10$ Gb/s) modulation and data transmission capabilities.

Today's commercially available high-speed optical modulators at $\gg 10$ Gb/s are based on electro-optic materials such as lithium niobate [16] and III-V semiconductors [17]. These devices have demonstrated modulation capability as high as 40 Gb/s. To achieve fast modulation in silicon is challenging, however, due to the fact that crystalline silicon exhibits no linear electro-optic (Pockels) coefficient and very weak Franz-Keldysh effect [18, 19].

Although it has been very recently shown that strained silicon possesses the Pockels effect [20], the measured electro-optic coefficient is relatively small (an order of magnitude smaller than that for LiNbO_3). It has also been shown that strained Ge/SiGe quantum well structures have relatively strong electro-optic absorption due to the quantum-confined Stark effect [21], making it possible for optical modulation. However, critical strain engineering is needed and optical modulator performance has yet to be demonstrated for the Ge quantum well system. To date, high speed modulation in silicon has only been demonstrated via the free carrier plasma dispersion effect [2, 3].

In silicon, free carrier density change results in a change in the refractive index of the material; therefore, the modulation speed of a silicon modulator based on the free carrier plasma dispersion effect is determined by how fast the free carriers can be injected or removed. Three different device configurations, namely, forward biased p-i-n diode [18, 19, 22], MOS capacitor [1, 2], and reverse biased pn junction [3, 23] have been proposed to achieve phase modulation in silicon. The forward biased p-i-n diode approach has been proven to provide high modulation efficiency (in turn compact device size [24]). However, due to the slow carrier generation and/or recombination processes, the modulation speed is usually limited unless the carrier lifetime can be significantly reduced [25]. While both MOS capacitor and reverse biased pn junction rely on electric-field induced majority carrier dynamics that can potentially achieve >10 Gb/s operation, one would need to adopt appropriate device design to improve the phase modulation efficiency. In addition, appropriate electrical driving schemes and resistance capacitance (RC) limitations have to be taken into account to reduce the device parasitic effects on the high frequency response of the device. We note that optical modulation based on free carrier effects in III-V semiconductors has also been investigated previously [26, 27]. It was suggested that the device speed for a reverse-biased pn junction is only limited by the RC constant.

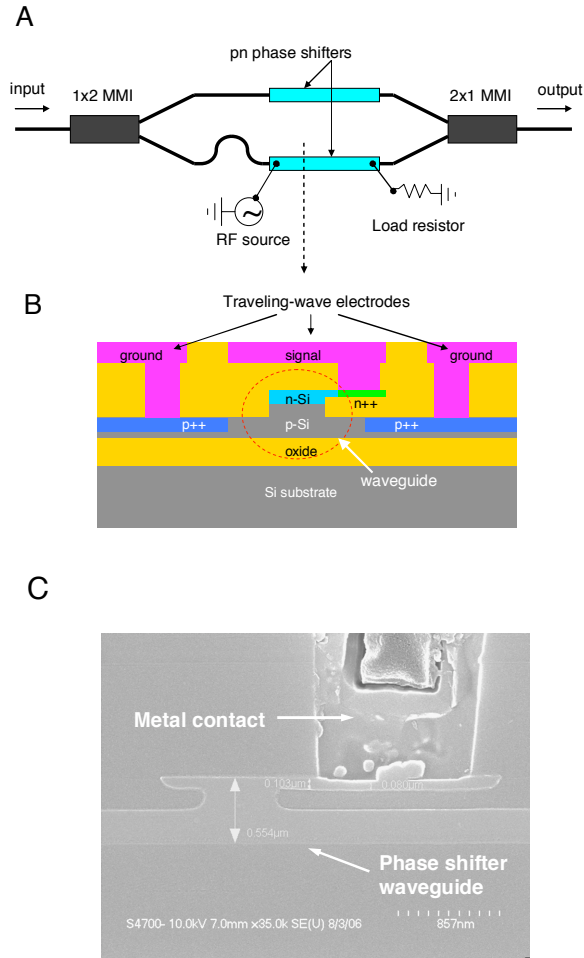


Fig. 1. (A) Top view of an asymmetric Mach-Zehnder interferometer silicon modulator containing two pn junction based phase shifters. The waveguide splitter is an 1x2 multi-mode interference (MMI) coupler. The RF signal is coupled to the travelling wave electrode from the optical input side and termination load is added to the output side. (B) Cross-sectional view of a pn junction waveguide phase shifter in Silicon-On-Insulator. The coplanar waveguide electrode has a signal metal width of $\sim 6 \mu\text{m}$ and a signal-ground metal separation of $\sim 3 \mu\text{m}$. The metal thickness is $\sim 1.5 \mu\text{m}$. The high-frequency characteristic impedance of the travelling wave electrode is $\sim 20 \Omega$. (C) Scanning electron microscope (SEM) image of a pn diode phase shifter waveguide.

2. Device design and fabrication

The high-speed silicon modulator presented here is based on a Mach-Zehnder interferometer (MZI) with a reverse biased pn diode embedded in each of the two arms, as shown in Fig. 1(a). To obtain better phase modulation efficiency, we designed and fabricated a sub-micrometer size waveguide. The silicon rib waveguide width is $\sim 0.6 \mu\text{m}$, rib height is $\sim 0.5 \mu\text{m}$, and etch depth is $\sim 0.22 \mu\text{m}$. Both modelling and experiment confirm that the waveguide is a single mode device for wavelengths around $1.55 \mu\text{m}$. The waveguide splitter is an 1x2 multi-mode interference (MMI) coupler. The MMI coupler is used because it has a broader range of operating wavelengths and larger fabrication tolerance as compared to a directional coupler. Also, because of the small waveguide dimensions, a conventional Y-junction would

have higher transmission loss. The asymmetric MZI arm design is used to simplify optical characterization and is not necessary for device operation. The MZI modulator with balanced arms has a broad bandwidth and can operate at 1.3 and 1.55 μm wavelength bands. The key active component of the silicon modulator is the reverse biased pn junction phase shifters embedded in the MZI arms. Figure 1(b) shows a schematic of the cross sectional view of the phase shifter. It comprises a p-type doped crystalline silicon rib waveguide having a rib width of $\sim 0.6 \mu\text{m}$ and a rib height of $\sim 0.5 \mu\text{m}$ with an n-type doped silicon cap layer ($\sim 1.8 \mu\text{m}$ wide). This thin ($\sim 0.1 \mu\text{m}$ thick) cap layer is formed using a non-selective epitaxial silicon growth process and is used for pn junction formation and electrical contact. The p-doping concentration is $\sim 1.5 \times 10^{17} \text{ cm}^{-3}$, and the n-doping concentration varies from $\sim 3 \times 10^{18} \text{ cm}^{-3}$ near the top of the cap layer to $\sim 1.5 \times 10^{17} \text{ cm}^{-3}$ at the pn junction. To insure good Ohmic contact between silicon and metal contacts, two slab regions $\sim 1 \mu\text{m}$ away from both sides of the rib edge and the thin cap layer $\sim 0.3 \mu\text{m}$ away from the rib edge are heavily doped with a dopant concentration of $\sim 1 \times 10^{20} \text{ cm}^{-3}$. The process is designed to target the pn junction at approximately $0.4 \mu\text{m}$ above the buried oxide to enable optimal modal overlap with the depletion region. As the n-doping concentration is much higher than the p-doping concentration, carrier depletion under reverse bias occurs mainly in the p-type doped region. This leads to better phase modulation efficiency because the hole density change results in a larger refractive index change as compared to the electron density change according to Kramers-Kronig analysis of optical absorption spectrum [18, 19].

Although it has been shown by 2D device simulation that the pn junction based silicon modulator has a fast intrinsic response (the transverse response time is $\sim 7 \text{ ps}$) [23], to experimentally demonstrate high frequency operation it is essential to overcome the issues associated with the relatively large pn junction capacitance and metal contact parasitics. To minimize the RC limitation of the frequency response of the modulator [28, 29], we designed a travelling wave electrode based on coplanar waveguide structure as shown in Fig. 1(b). The single sided asymmetric silicon cap layer design is used to reduce the capacitance of the phase shifter. The “signal” metal layer is $\sim 6 \mu\text{m}$ wide and is connected to the n-type silicon region through a $1 \mu\text{m}$ contact. The separation between the signal and ground metal layers is $\sim 3 \mu\text{m}$ and the metal thickness is $\sim 1.5 \mu\text{m}$. The RF travelling wave coplanar waveguide and modulator optical waveguide are carefully designed so that both electrical and optical signals co-propagate along the length of the phase shifter with similar speeds, while, at the same time, the RF attenuation is kept to be as small as possible. The transmission line loss, impedance, and phase velocity were calculated by using a commercial software package HFSS. These parameters strongly depend on the metal trace dimensions as well as silicon doping concentration and profile. The cross-section scanning electron microscope (SEM) image of a fabricated pn diode phase shifter waveguide is shown in Fig. 1(c).

For a reverse biased pn junction, the depletion width depends on the bias voltage and doping concentrations. For the asymmetrically doped pn junction in this work (the n-doping concentration is much higher than the p-doping concentration), the depletion width (W_D) can be approximated by [30]

$$W_D = \left(\frac{2\epsilon_0\epsilon_r(V_{Bi} + V_{app})}{eN_A} \right)^{1/2} \quad (1)$$

where ϵ_0 and ϵ_r are the vacuum permittivity and low-frequency relative permittivity of silicon, e is the electron charge, N_A is the acceptor concentration, V_{Bi} is the built-in voltage, and V_{app} is the applied voltage. Changing the depletion width of a pn junction is equivalent to

changing the free carrier density. Thus, by changing the bias voltage, one can achieve refractive index modulation through the free carrier plasma dispersion effect. Because the depletion width is usually smaller than the waveguide height, the phase modulation efficiency strongly depends on the pn junction location.

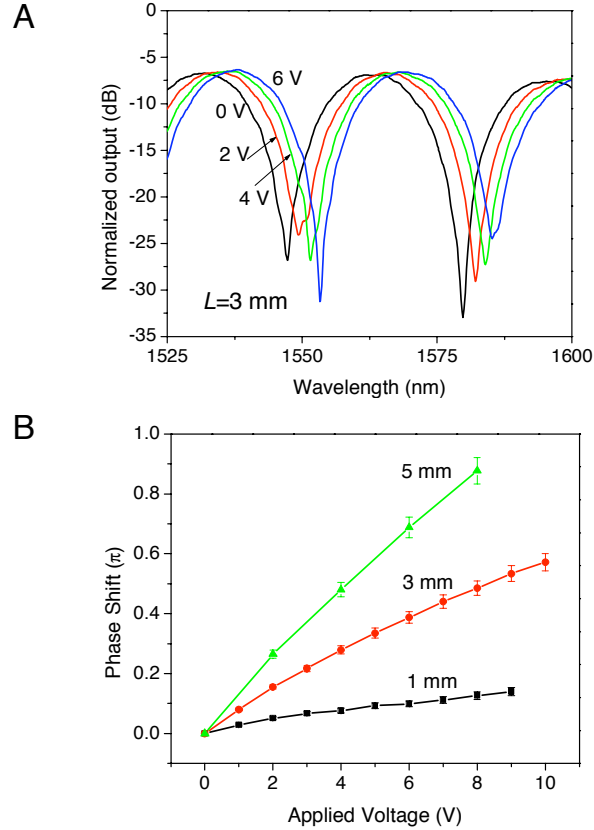


Fig. 2. (A) The output spectra of a MZI modulator having 3 mm long phase shifters for various voltages applied to one of the arms. The MZI output is normalized to the output of a straight waveguide with the same waveguide length without pn junction and drive voltage. (B) The phase shift of an individual phase shifter vs. the drive voltage for the wavelength round 1550 nm for different phase shifter lengths.

3. Device characterization

We characterize the phase efficiency of the pn junction phase shifter using an asymmetric MZI with a built-in arm length difference of ~ 20 μ m. Because of this waveguide length difference, the MZI output intensity depends on both the wavelength and the phase modulation induced by the bias voltage. Figure 2(a) shows the measured output spectra of an MZI modulator with 3 mm long phase shifters for various DC voltages applied to one of the arms. As expected from the bias-induced increase in the effective refractive index of the phase shifter, the MZI output spectrum shows a red-shift with increasing applied voltage. It can also be seen from Fig. 2(a) that the DC extinction ratio of the MZI modulator is >20 dB over a wide wavelength range. The on-chip insertion loss is ~ 7 dB when the MZI is in the “on” state, which is defined here as the maximum optical output intensity of the MZI. This on-chip insertion loss (excluding coupling loss) includes ~ 1 dB passive waveguide transmission loss, ~ 0.5 dB MMI coupler loss, and ~ 5.4 dB phase shifter loss, which can be attributed primarily

to the dopants. The passive waveguide and phase shifter losses are measured using the well-known cutback method [31], and the MMI coupler loss is determined by comparing its transmission to that of straight reference waveguides.

As the refractive index change is very weakly dependent on the wavelength in the wavelength range used in Fig. 2(a), the voltage-induced wavelength shift ($\Delta\lambda$) in the MZI output spectrum can be used to extract the voltage-induced phase shift ($\Delta\phi$) using the relationship $\Delta\phi = 2\pi\Delta\lambda / FSR$, where FSR is the free spectral range of the asymmetric MZI. For the device design used in this work, FSR is measured to be ~ 32 nm, which is in good agreement with the modelled value of 31.7 nm. Figure 2(b) shows the measured phase shift of the pn junction phase shifter as a function of the drive voltage for different phase shifter lengths. As the data shows, $\pi/2$ phase shift is achieved at 4 V bias for a phase shifter length of 5 mm. As a figure of merit for phase modulation efficiency, $V_\pi L$ (where V_π is the bias voltage required for π phase shift and L is the device length) is ~ 4 V.cm for our pn junction phase modulator. We see from Fig. 2(b) that the phase shift is not linearly dependent on the drive voltage, which is expected because the depletion width is not linearly dependent on voltage [see Eq. (1)].

The high frequency performance of the silicon modulator is characterized by measuring both its 3 dB frequency roll-off and data transmission capability. To enable high speed testing, the silicon MZI modulator chip is flip-chip bonded to a printed circuit board (PCB) with low RF loss connectors. The PCB is also designed for high speed performance with PCB traces having ~ 0.3 dB/cm RF loss at 40 GHz. The MZI silicon modulator used for the high speed experiments contains an 1 mm long pn junction phase shifter in each arm. Although one could drive both arms in push-pull configuration, the high speed testing is performed using a single-ended drive scheme. Figure 3 shows a schematic of the experimental setup used for the high-speed measurements. First, the RF signal from either a signal generator or a pseudo-random bit sequence (PRBS) generator is amplified using a commercially available modulator driver. The amplified output of ~ 6.5 V_{pp} is combined with 3.5 V_{DC} using a bias Tee to ensure reverse bias operation for the entire AC voltage swing. This DC-coupled signal is connected to the input of the travelling-wave electrode of one of the phase shifters via the PCB connector. The output of the electrode is terminated with a 20 Ω load. A continuous-wave laser beam at ~ 1550 nm is coupled into the silicon modulator via a lensed fiber. The modulated optical output is collected using another lensed fiber and is connected to a digital communications analyzer (DCA) optical module with a 53 GHz photo-receiver.

For the optical frequency roll-off measurement, the signal generator is swept from 100 MHz to 40 GHz. The DC-coupled signal after the bias Tee, which is also the drive signal or input voltage for the silicon modulator at PCB input connector, is first measured as a function of frequency using a DCA electrical module with 63 GHz bandwidth. Then this RF signal is connected to the PCB to drive the modulator. The modulated optical signal is also measured as a function of frequency. To obtain the frequency response of the MZI modulator for a constant input drive voltage, the photo-receiver output is normalized by the input drive voltage for all frequencies. The resulting data is given in Fig. 4(a), which shows that the MZI modulator has a 3-dB roll-off frequency of ~ 20 GHz.

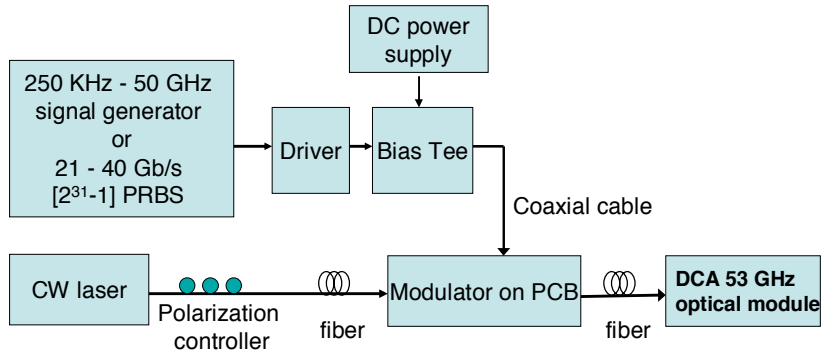


Fig. 3. Experimental setup for MZI high speed optical frequency response and data transmission measurements.

We also investigated the high speed data transmission performance of the MZI modulator. The experimental setup is shown in Fig. 3, and its only difference compared to that used for the roll-off measurement is that a PRBS with $[2^{31}-1]$ pattern length is used as the RF source. Figure 4(b) shows the modulator optical eye diagram at a bit rate of 30 Gb/s. The open eye diagram suggests that the modulator is capable of transmitting data at 30 Gb/s, which is consistent with the 3 dB roll-off frequency of ~ 20 GHz. Such high speed data transmission represents a significant leap in silicon modulator performance in reference to the previously published work [2, 3].

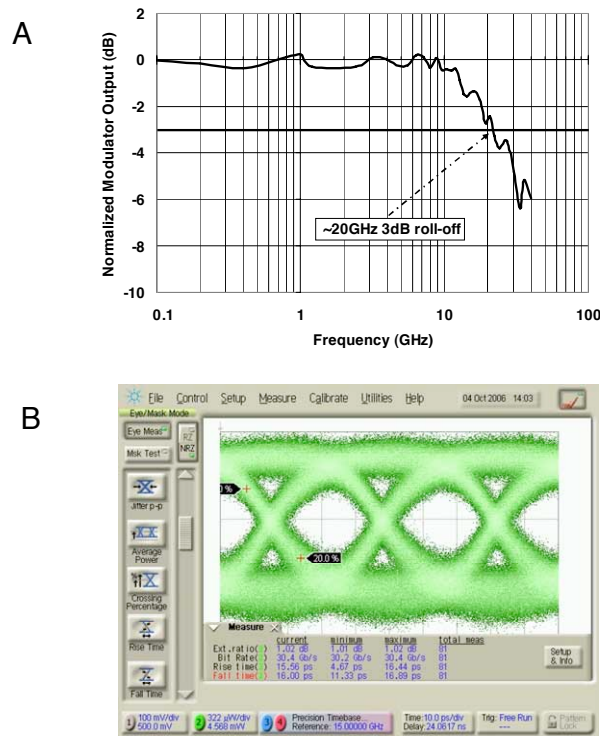


Fig. 4. (A) Optical response of a silicon modulator as a function of the RF frequency for a MZI having 1 mm long phase shifter. (B) Optical eye diagram of the MZI modulator having a 1 mm long phase shifter. The bit rate is 30 Gb/s.

4. Discussion and conclusion

Although we have demonstrated high speed operation of the MZI with a 3 dB roll-off frequency of ~ 20 GHz, the current silicon modulator is by no means optimized for performance. For example, the device can be improved by optimizing the dopant profile and pn junction placement in the waveguide to increase phase efficiency. This would reduce the $V_{\pi}L$ of the current modulator by a factor of ~ 2 according to simulations. By operating the MZI in a push-pull configuration [2, 32, 33] ($\pi/2$ phase shift is required in each arm), one would be able to further reduce the drive voltage by a factor of 2. As the reverse biased pn diode modulator has a fast intrinsic speed of 40 GHz and beyond [23], its bandwidth can be scaled by lowering the RF loss of the travelling-wave electrode, better matching driver/modulator transmission line impedance, and optimizing the travelling-wave electrode termination circuitry. In addition, insertion loss of the MZI modulator can be reduced by using the lower loss approach of selective epitaxial growth [34] of silicon for the n-type silicon cap layer above the rib, as opposed to the non-selective epitaxial silicon used in the current modulator. By optimizing the n-doping concentration and profile, our modelling suggests that the phase shifter loss could be reduced to 2 dB from 5.4 dB obtained for the current 3 mm long phase shifter. Finally, by adding silicon tapers to the waveguide input and output, one can achieve efficient fiber coupling to the modulator structure.

In conclusion, we have presented design, fabrication, and characterization of a high-speed silicon optical modulator. The silicon modulator is based on electric-field-induced carrier depletion effect in a Silicon-on-Insulator waveguide containing a reversely biased pn junction. The high-frequency performance was characterized with both optical response frequency roll-off and data transmission measurements. We demonstrated a silicon modulator with a 3 dB bandwidth exceeding 20 GHz and data transmission of 30 Gb/s. This unprecedented leap in data transmission will enable silicon modulator to be one of the key building blocks for future highly integrated silicon photonic chips and architectures capable of transmitting data at Tb/s.

Acknowledgments

The authors thank K. Callegari and J. Tseng for sample preparation, T. Luo for early work on RF characterization, D. Li for data collection software, R. Cohen, R. Gabay, A. Ugnitz, and G. Nutrica for device fabrication assistance, L. Kulig for material analysis, and T. Mader, S. Q. Shang, G. Sarid, T. Franck, R. Jones, D. D. Lu, H. Braunisch, G. T. Reed, and J. E. Bowers for useful discussions.